ELSEVIER

Contents lists available at ScienceDirect

Corrosion Communications

journal homepage: www.elsevier.com/locate/corcom



Research Article

Manipulation of Cr interlayer in amorphous carbon coating for anti-tribo-corrosion behavior



Guanshui Ma^a, Jiangshan Yan^{a,b}, Naiming Lin^{b,*}, Peng Guo^a, Wei Yang^a, Changying Chen^a, Aiying Wang^{a,*}

- ^a State Key Laboratory of Advanced Marine Materials, Zhejiang Key Laboratory of Extreme-environmental Material Surfaces and Interfaces, Ningbo Institute of Materials Technology and Engineering, Chinese Academy of Sciences, Ningbo 315201, China
- ^b College of Materials Science and Engineering, Taiyuan University of Technology, Taiyuan 030024, China

ARTICLE INFO

Article history:
Received 17 July 2024
Received in revised form 29 August 2024
Accepted 5 September 2024
Available online 31 July 2025

Keywords: 316L stainless steel Graphite-like carbon coatings Cr interlayer Tribo-corrosion performance

ABSTRACT

316L stainless steel (316L) is widely recognized as the primary structural material employed in offshore equipment. However, it is prone to damage from both abrasion and corrosion (tribo-corrosion) when exposed to the marine environment. In this study, graphite-like carbon (GLC) coatings with varying thicknesses of chromium (Cr) interlayer were employed to enhance the tribo-corrosion performance of 316L. The results revealed that all the GLC coatings exhibited remarkable tribo-corrosion performance in a 3.5 wt.% NaCl solution. Notably, the thickness of the Cr interlayer has minimal impact on the tribo-corrosion performance under a 5 N load. This is primarily because the surface GLC layer plays a predominant role in influencing the behavior under this load condition. However, under a 40 N load, the thickness of the Cr interlayer has a significant impact on the tribo-corrosion performance, which is attributed to the vital role played by the Cr interlayer in terms of adhesion strength and bearing capacity. Among the tested GLC coatings, the one with a Cr interlayer thickness of 575 nm exhibits the best tribo-corrosion performance, suggesting that an appropriate thickness of the Cr interlayer can provide the highest wear resistance under high load. The work provides fundamental insight into the electrochemical corrosion and tribological behavior of GLC coatings in harsh marine applications.

© 2025 The Author(s). Published by Elsevier B.V. on behalf of Institute of Metal Research, Chinese Academy of Sciences.

This is an open access article under the CC BY-NC-ND license (http://creativecommons.org/licenses/by-nc-nd/4.0/)

1. Introduction

With the rapid advancement in the exploration of marine resources, the demand for modern marine engineering equipment has been steadily increasing [1,2]. One commonly used material for structural components and moving parts in such equipment is 316L stainless steel (316L) due to its excellent resistance to Cl⁻ corrosion, impressive mechanical properties, favorable formability and weldability, and reasonable cost [3,4]. However, corrosion and wear have emerged as the most critical concerns faced by moving engineering equipment operating in harsh and complex marine environments [5–8]. These issues can result in component failure and pose a threat to the overall service life of the equipment. Previous work has demonstrated that friction accelerates corrosion in the wear track area, and as the applied potential increases, the wear loss also increases in artificial seawater [9–11]. We also conducted a study on the tribo-corrosion behavior of 316L in simulated seawater

under sliding at open circuit potential (OCP), and the results revealed that accelerated damage to 316L under sliding was attributed to periodic mechanical removal of the thickened passive film and promoted abrasive wear within the wear track [12,13].

Given the harmfulness of this phenomenon, researchers have developed a range of protective coatings, such as amorphous carbon (a-C) coatings [14–17], metal coatings [18], and ceramic coatings [19,20], to enhance the abrasion and corrosion resistance of 316L. Among them, graphite-like carbon (GLC, sp² dominate), a type of a-C with predominantly sp² configuration, has garnered significant attention due to its low coefficient of friction (COF), exceptional chemical stability in seawater environments, and unique layered structure [21–27]. GLC coatings have been recognized as one of the most promising options for improving the tribological and anti-corrosive properties of metallic substrates, thereby extending the lifespan of components used in marine engineering equipment [28,29]. However, most tribological and anti-

E-mail addresses: linnaiming@tyut.edu.cn (N. Lin), aywang@nimte.ac.cn (A. Wang).

^{*} Corresponding authors.

corrosive behaviors of GLC coatings exhibit a strong dependence on their residual stress, poor adhesion strength and abundant surface defects, which are closely related to the interface between the coatings and the substrates [30–32].

It is well known that the metal interlayer between the coating and substrate can mitigate performance differences and extend the diffusion path of corrosive media, thus improving the coating's performance [33-36]. The optimization of interlayer thickness is particularly critical when considering a-C films, as it directly influences their performance. Shi et al. [37] studied the effect of interlayer thickness on microstructure, mechanical, tribological and corrosion behavior of the GLC films. Their findings revealed a consistent decrease in mechanical properties and bonding strength as the interlayer thickness increased, which was attributed to an increase in sp2 content, surface roughness, and a concurrent decrease in film integrity, consequently leading to reduced wear resistance in both ambient air and NaCl solution. Chen et al. [38] shed light on the influence of SiN_x interlayer thickness on the microstructure, adhesion, and tribological properties of DLC coatings. Remarkably, they observed a non-linear trend whereby an initial decrease in internal stress and surface roughness was followed by a subsequent increase with increasing interlayer thickness. Notably, the coating with an interlayer thickness of 10 nm displayed the optimum tribological and mechanical properties, owing to the aggregation of nitrogen-vacancy centers. Furthermore, the specific choice of interlayer has a distinct impact on the performance of the outermost coatings. Wang et al. [39] examined the effects of various interlayers, including single Ti, single Cr, thickness gradient Cr/C, and composition gradient Cr/C on the performance of GLC films. The results exhibited substantial improvements in adhesion strength and load-bearing capacity under sliding-friction conditions in water through interlayer design. GLC films with a composition gradient Cr/C interlayer demonstrated the highest adhesion strength and loadbearing capacity, which could be ascribed to the presence of a nanointerlocked microstructure and the formation of hard carbide phases within the interlayer. In our previous report [40,41], we also compared the influence of the Ti, W and Cr inlayers on the performance of GLC, and the results demonstrated that the Cr interlayer promoted the graphitization degree of the tribo-film and provided GLC with the best frictional and electrochemical properties.

In practice, the incorporation of a metal interlayer typically enhances the operational performance of carbon-based coatings. However, an increase in the thickness of the layer often results in the formation of a coarse columnar crystal structure, which can diminish the bonding at the interface between the metal and GLC, as well as reduce the compactness of the GLC. Conversely, when the metal interlayer is excessively thin, it may exist in the form of fine grains, facilitating stronger interface bonding and a higher density of the GLC, which can pose challenges in achieving adequate abrasion protection under high loads. The key is-

sue in this field is thus to optimize the thickness of the metal interlayer and to effectively design abrasion-resistant coatings that can perform optimally under varying contact stress.

In the present work, GLC coatings with different thicknesses of Cr interlayer were successfully deposited on 316L by direct current magnetron sputtering (DCMS) technique. The influence of the Cr interlayer with different thicknesses on the structure, composition and adhesion strength of the surface GLC was studied. Especially, the tribo-corrosion behavior in 3.5 wt.% NaCl solution under different loads (5 and 40 N) was investigated, and the related tribo-corrosion failure mechanism was also discussed in detail. The purpose is mainly to explore a solution to the long-term tribo-corrosion application of GLC films under marine environments and to fill the research gap on the effect of interlayer thickness on the properties of GLC coating.

2. Experimental

2.1. Sample preparation

316L in the size of Φ 17 mm \times 3 mm and a Si wafer were used as substrates. Before deposition, the samples underwent two rounds of ultrasonic cleaning in acetone and were subsequently cleaned in ethanol for 10 min. After the cleaning process, the samples were placed into the deposition chamber. When the base vacuum reached 6.67×10^{-3} Pa, the substrate was etched by Ar ions for 10 min. Cr interlayer was deposited using a Cr (380 mm \times 100 mm \times 7 mm, 99.99 wt.%) target with the sputtering current of 3.0 A, and a bias of -100 V. The thickness of the Cr interlayer was controlled by adjusting the deposition time, resulting in four samples referred to as Cr-0, Cr-1, Cr-2, and Cr-3, corresponding to deposition times of 0, 7, 15, and 22 min, respectively. GLC coating was deposited by a graphite (380 mm \times 100 mm \times 7 mm, 99.99 wt.%) target with a sputtering current of 3.0 A, a bias voltage of -200 V. The deposition time of the GLC coating was 120 min. The sample holder rotated at a constant speed of 10 r/min to maintain the uniformity of the coatings during deposition. The schematic diagram of the DCMS system is shown in Fig. 1(a).

2.2. Microstructural characterizations

The surface morphology, thickness of the deposited GLC coatings, morphology and component of wear track were investigated by scanning electron microscopy (SEM, Verios G4 UC) with an energy dispersive X-ray (EDX) analyzer at 15 kV. Microstructure of deposited coatings was measured by Renishaw in Via Reflex confocal Raman spectroscopy, employing a wavelength of 532 nm. The bonding state of GLC coatings was analyzed by X-ray photoelectron spectroscopy (XPS, AXIS SUPRA).

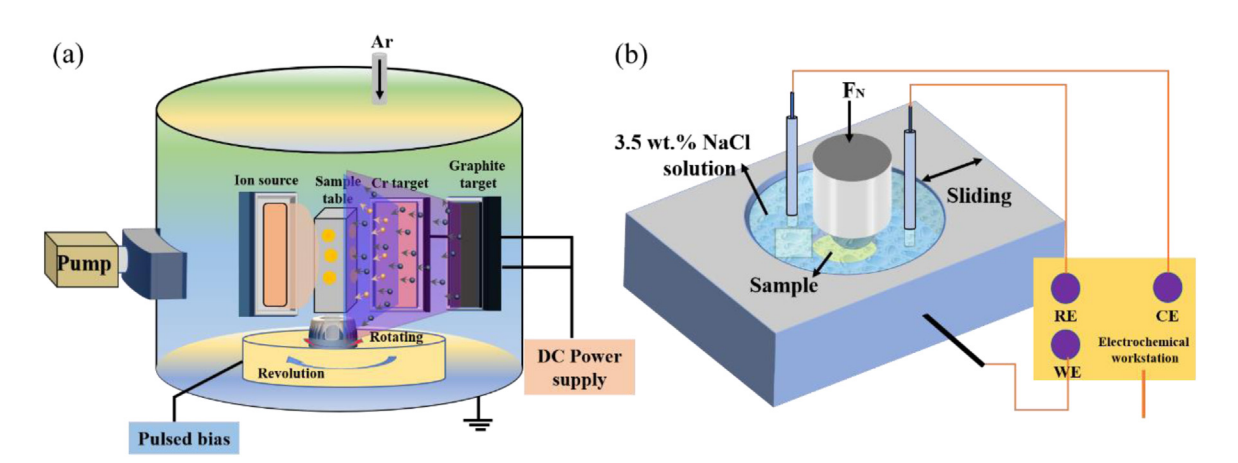


Fig. 1. (a) Schematic diagram of the DCMS system for sample deposition and (b) tribo-corrosion equipment.

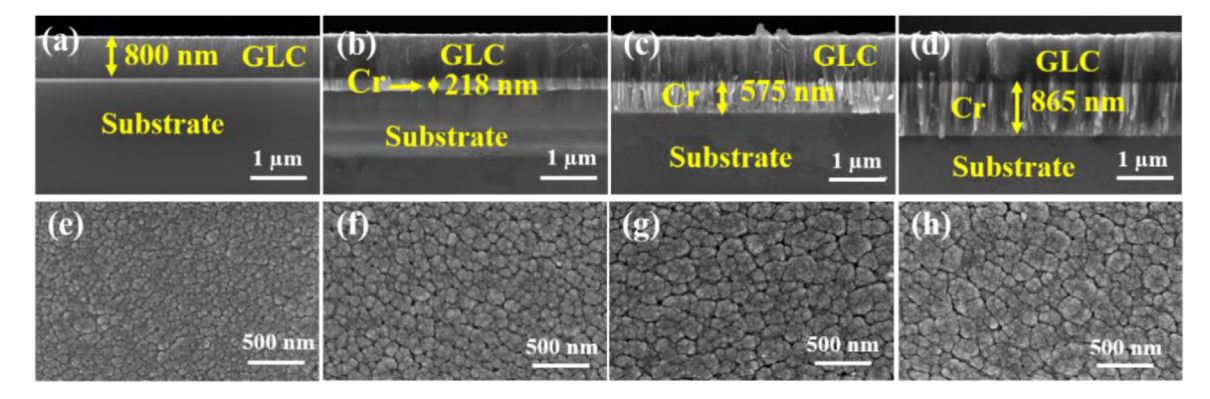


Fig. 2. (a-d) Cross-sectional and (e-h) surface morphologies of (a, e) Cr-0, (b, f) Cr-1, (c, g) Cr-2 and (d, h) Cr-3.

2.3. Tribo-corrosion performance

Tribo-corrosion tests were conducted in 3.5 wt.% NaCl solution using a ball-on-disk reciprocating tribometer (Rtec). The tribometer was connected with a three-electrochemical cell (Mudulab) to collect the OCP of the samples at room temperature. A platinum electrode was used as the counter electrode (CE), a saturated calomel electrode (SCE) was used as the reference electrode (RE), and samples were used as the working electrode (WE), as shown in Fig. 1(b). For the tests, $\mathrm{Si}_3\mathrm{N}_4$ balls with a diameter of 6 mm were employed as the friction counterpart. The sliding tests were conducted at a rate of 20 mm/s, with a stroke length of 4 mm, and an exposed area of 2 cm². Two different normal loads were selected: 5 N (the maximum contact stress σ_{max} : 410 MPa) and 40 N (σ_{max} : 820 MPa). The sliding time under the 5 N was 60 min and the longest sliding time under the 40 N was 300 min. σ_{max} is calculated using the following formula [42]:

$$\sigma_{\text{max}} = \sqrt[3]{\frac{3FR}{4E}} \tag{1}$$

where F is the concentrated load (N), E represents the modulus of elasticity (MPa) and E is the radius of the Si₃N₄ ball (mm).

3. Results and discussion

3.1. Microstructure of coatings

Fig. 2 illustrates the cross-sectional and surface morphologies of the GLC coatings with varying thicknesses of Cr interlayer. The distinct boundaries between the Cr and GLC layers indicate a strong bond with the substrate. The thickness of the GLC coatings is approximately 800 nm, while the thicknesses of Cr interlayer are measured at around 218, 575, and 865 nm, respectively. This implies that the

thickness of the Cr interlayer is determined by the deposition time accurately. Analysis of the cross-sectional morphologies reveals a more pronounced columnar structure with increasing the thickness of Cr interlayer, confirming the significant influence of interlayer thickness on the coating structure, as previously reported [43,44]. Additionally, the surface of the coatings displays the gradual growth of large clusters composed of fine particles with prolonged interlayer sputtering time. This observation further exemplifies the effective role of the Cr interlayer in promoting the adsorption and nucleation of the GLC coatings.

To examine the influence of Cr on the structure of GLC, Fig. 3(a) displays the Raman spectra and corresponding Gaussian fitting results for the Cr-0, Cr-1, Cr-2, and Cr-3 coatings. It is evident that the Raman spectra obtained from all samples exhibit a broad and asymmetric Raman scattering band within the range of 900–1800 cm⁻¹. The band can be fitted with two Gaussian peaks, denoted as the D and G peaks, which correspond to the stretching and breathing vibration of the carbon ring, respectively [45]. It is generally accepted that the G-peak positions, the peak area ratio of D-peak to G-peak $(I_{\rm D}/I_{\rm G})$ and full width at half maximum of G-peak ($G_{\rm FWHM}$) of GLC coatings are widely accepted as indirect indicators of the \mbox{sp}^2/\mbox{sp}^3 ratio, bond disorder and \mbox{sp}^2 cluster size of GLC coatings [14,46]. Seen from Fig. 3(b), upon the addition of Cr interlayers, the I_D/I_G decreases from 3.69 to around 3.16. This decrease signifies that the introduction of Cr affects the sp²/sp³ ratio. Previous studies have also proposed that this phenomenon can be attributed to the catalysts in the metal buffer, which play a role in the formation of sp² structures [47,48]. The position of the G peak remains stable around 1550 cm⁻¹, suggesting that the bond disorder undergoes minimal change. In comparison to other samples, the Cr-2 exhibits the lowest G_{FWHM} of 159 cm⁻¹, indicating that the thickness of the transition Cr layer also influences the size of sp² clusters, which is similar to the previous reports [44].

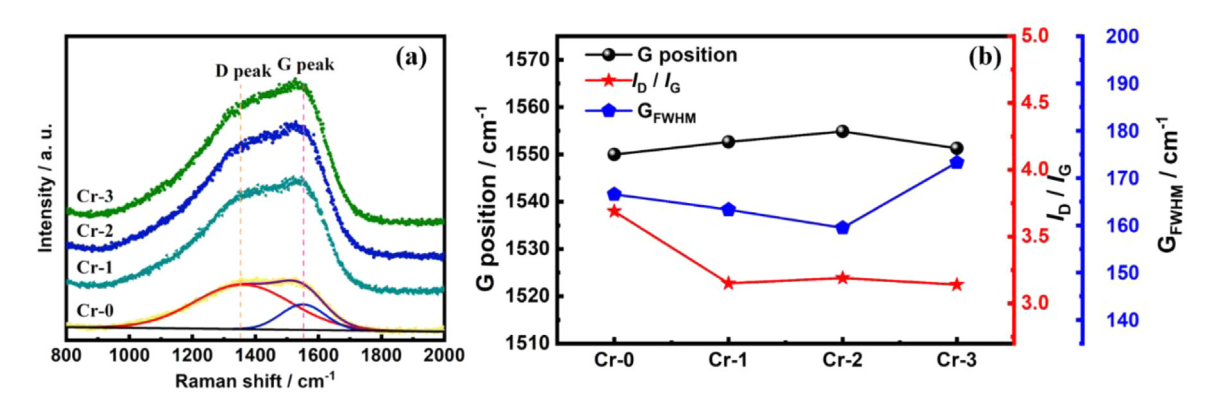


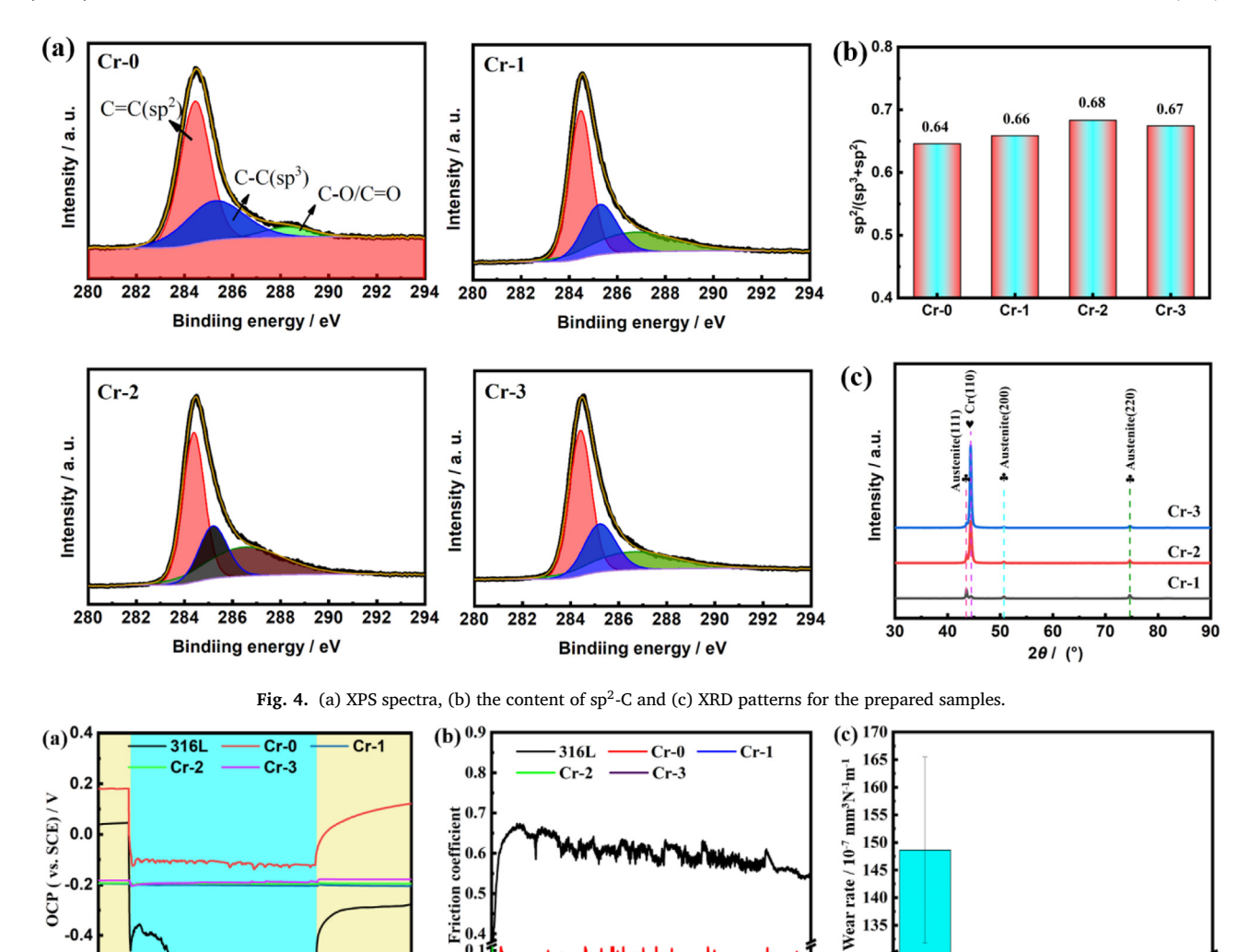
Fig. 3. (a) Raman spectra and (b) the fitted G-peak position, I_D/I_G , G_{FWHM} of the Cr-0, Cr-1, Cr-2 and Cr-3.

0.0

-0.2

-0.4

10 20 30



Friction 0.5

50

60

composition of the prepared coatings. Fig. 4(a) presents the C 1s spectrum, revealing three distinct peaks. The peak at 284.5 eV corresponds to sp²-C, while the peak at 285.3 eV represents sp³-C. The presence of C-O/C = O peaks around 288.1 eV can be attributed to prolonged exposure to air or potential oxygen incorporation during the film deposition process [35,49]. In Fig. 4(b), as the thickness of the Cr interlayer increased, the relative content of sp2-C hybrid bonds increased slightly from about 0.64 to 0.68, and then decreased to 0.67, indicating that Cr interlayer could promote the graphitization of GLC coating, which was consistent with the results of Raman. The crystalline phases of the prepared samples are also characterized by XRD, as indicated in Fig. 4(c). The XRD patterns display two crystalline phases, corresponding to 316L austenite (PDF#47-1417) and Cr (PDF#06-0694). As the Cr thickness increases, the diffraction peak intensity of the 316L austenite phase gradually diminishes, while the (100) plane of Cr around 44.39°

XPS analysis was employed to further characterize the sp² and sp³

40 50 60

Time / min

70 80 90 100

10

20

30

40

Fig. 5. Tribo-corrosion test results under 5 N in 3.5 wt.% NaCl solution: (a) OCP, (b) the calculated average coefficient of friction, (c) the wear rate.

3.2. Tribo-corrosion performance under 5 and 40 N

becomes more pronounced and sharper.

To investigate the tribo-corrosion behavior of GLC coatings with different thicknesses of Cr in seawater, tribo-corrosion experiments at OCP are conducted in 3.5 wt.% NaCl solution, with applied loads of 5 and 40 N, respectively. Fig. 5 displays the results of tribo-corrosion perfor-

mance for 316L, Cr-0, Cr-1, Cr-2 and Cr-3 coatings in 3.5 wt.% NaCl solution under a load of 5 N. In Fig. 5(a), the OCP of 316L initially drops greatly from 0.04 V to -0.53 V due to the damage or removal of the passive layer in the wear track. Then the OCP curve stabilizes throughout the test. After sliding, the OCP shifts to -0.3 V may be attributed to the repassivation of the worn surface [5]. For Cr-0, its OCP decreases from $0.18\ V$ to $-0.12\ V$ at the start of the test, which may be associated with the rupture or damage of the GLC coating. However, it remains relatively stable during the entire friction process [50]. On the other hand, Cr-1, Cr-2, and Cr-3 exhibit almost constant OCP throughout the test, indicating that the surface and electrochemical properties are less affected by friction under a load of 5 N. Fig. 5(b) shows that the COF decreases from 0.6 to 0.07 after the deposition of the GLC coating on 316L. Furthermore, the COF value for Cr-0 fluctuates during the entire friction process, possibly due to coating damage. In Fig. 5(c), the wear rates of the 316L, Cr-0, Cr-1, Cr-2 and Cr-3 are determined to be 1.486×10^{-5} , 5.19×10^{-7} , 2.13×10^{-7} , 1.52×10^{-7} , and 2.16×10^{-7} mm³/(N·m), respectively. Obviously, all the GLC coatings significantly reduce the wear rate of 316L. However, there is no significant difference in wear rates observed among Cr-1, Cr-2, and Cr-3 under a load of 5 N.

316L

Cr-0

Cr-1

Fig. 6 depicts the tribo-corrosion test results in 3.5 wt.% NaCl solution under 40 N. The tribo-corrosion performance of the 316L under 40 N is not analyzed because of its severe wear under 5 N. In respect of Fig. 6(a), the OCP curve of Cr-0 initialy drops significantly from

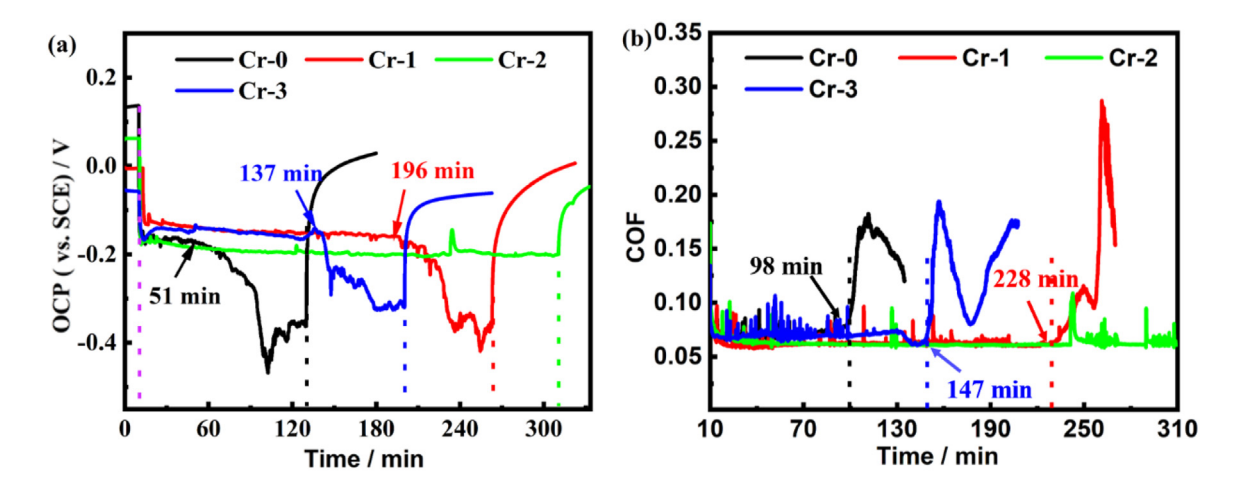


Fig. 6. Tribo-corrosion test results under 40 N in 3.5 wt.% NaCl solution: (a) OCP, (b) the calculated average coefficient of friction.

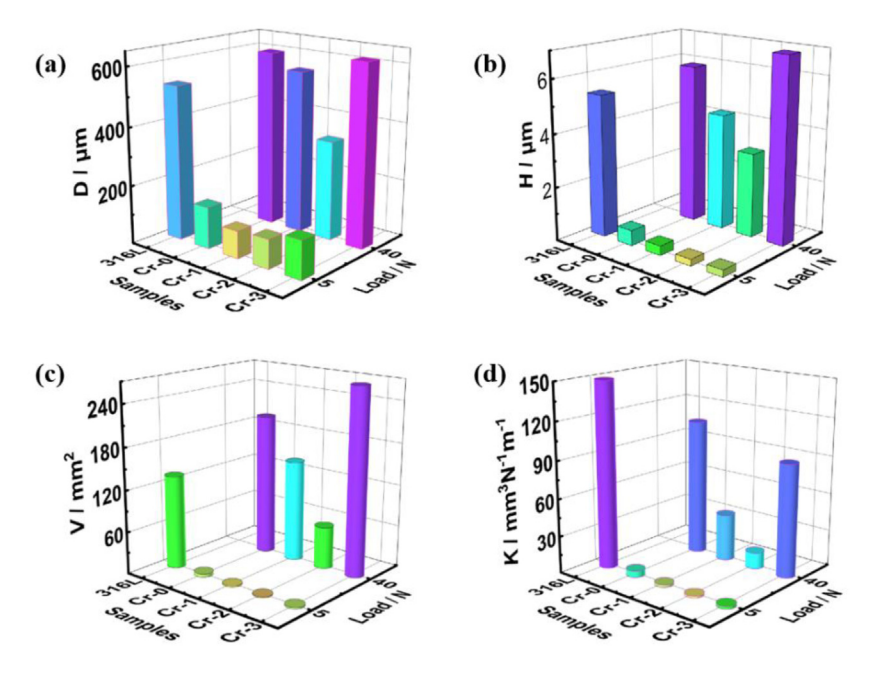


Fig. 7. Wear trace geometric parameters and wear rate of 316L, Cr-0, Cr-1, Cr-2 and Cr-3 after tribo-corrosion test: (a) D, (b) H, (c) V, (d) K.

0.13 V to -0.16 V and stabilizes for a short time. Subsequently, the OCP curve experiences a rapid decline at 51 min. Similar observations are obtained from Cr-1 at 137 min and Cr-3 at 196 min, which may be attributed to coating peeling [14]. However, for Cr-2, the OCP remains stable throughout the entire tribo-corrosion test, indicating the integrity of the coating. In Fig. 6(b), the COFs of all samples are initially relatively low, averaging around 0.067 ± 0.005 . Subsequently, the COFs for Cr-0, Cr-1, and Cr-3 begin to rise at 98, 228, and 147 min, respectively. In contrast, the COF of Cr-2 remains relatively stable. The earlier change in OCP compared to COF suggests that OCP is more sensitive to coating damage. Based on the COF and OCP curves, it can be reasonably inferred that the Cr-2 coating demonstrates good substrate protection and has a longer service life under a load of 40 N.

To systematically compare the damage inflicted on the 316L substrate and the Cr-0, Cr-1, Cr-2, and Cr-3 coatings under different loads (5 and 40 N), the width (*D*), depth (*H*), volume (*V*), and wear rate (*K*) of the wear tracks were systematically analyzed, as shown in Fig. 7. It is evident that all samples, except for 316L, exhibit smaller values for *D*, *H*, *V*, and *K* under 5 N load. However, when the load is increased from 5 N to 40 N, all samples, except for Cr-2, experience significant changes

in *D*, *H*, *V*, and *K*, indicating severe wear. In other words, the thickness of the Cr layer has minimal impact on the tribo-corrosion performance under 5 N but has a considerable influence under 40 N.

3.3. Wear track evolution after tribo-corrosion test

Fig. 8 illustrates the morphologies of the wear track of 316L, Cr-0, Cr-1, Cr-2 and Cr-3 after tribo-corrosion test under a load of 5 N. It is evident that 316L experiences severe abrasion, as seen in Fig. 8(a) and (ff), with a rough wear track containing numerous grooves parallel to the sliding direction. These coarse and uneven grooves contribute to the instability observed in the friction coefficient in Fig. 5(b). In addition, as shown in Fig. 8(b) and (g), the surface of Cr-0 appears relatively smooth, but some regions exhibit flaking, which confirms the observed fluctuation in the friction coefficient during the tribo-corrosion test. Notably, for Cr-1, Cr-2, and Cr-3 coatings, their wear tracks are smooth, with only slight cracks and a few grinding grooves visible on the surface of Cr-1. Similarly, Cr-2 and Cr-3 display shallower wear tracks. In general, the GLC coatings with Cr interlayer show better anti-tribo-corrosion performance, and the thickness of Cr layer has little effect on the tribo-

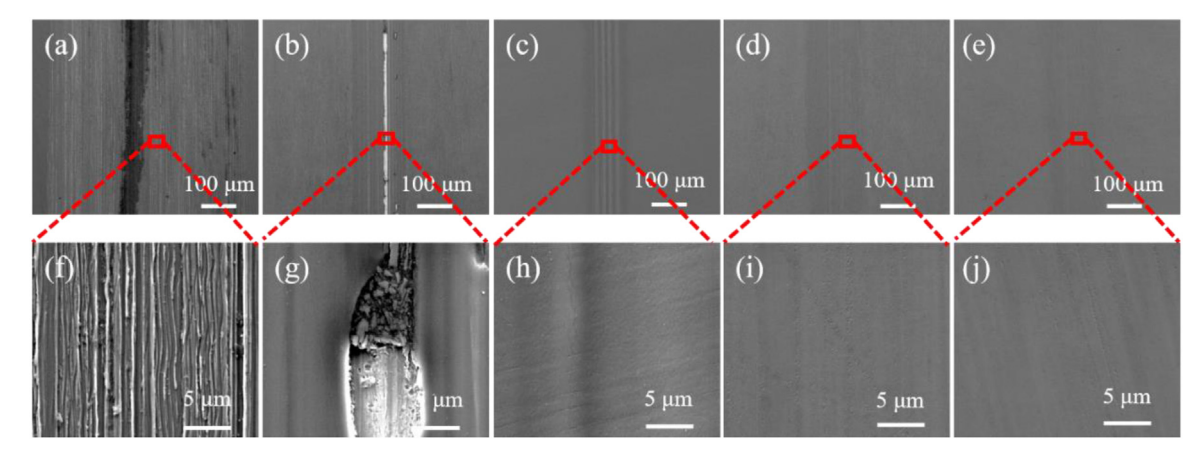


Fig. 8. Wear track of (a, f) 316L, (b, g) Cr-0, (c, h) Cr-1, (d, i) Cr-2, (e, j) Cr-3 after tribo-corrosion test with 60 min under load of 5 N in 3.5 wt.% NaCl solution.

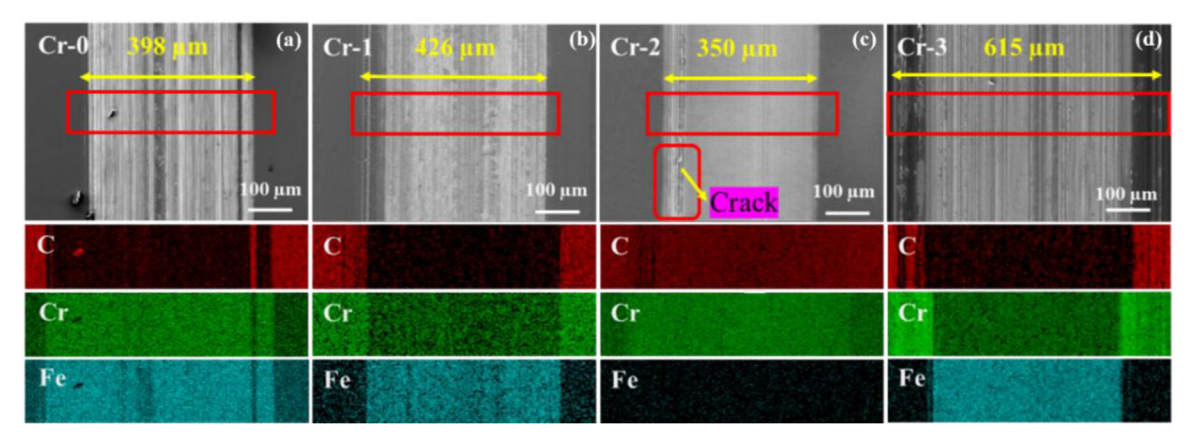


Fig. 9. Wear track and corresponded EDX mapping results of (a) Cr-0, (b) Cr-1, (c) Cr-2 and (d) Cr-3 after tribo-corrosion test under a load of 40 N in 3.5 wt.% NaCl solution.

corrosion performance under 5 N. The above results have provided a good explanation for the results of tribo-corrosion test.

The wear track morphologies and corresponded EDX of Cr-0, Cr-1, Cr-2 and Cr-3 after tribo-corrosion test under a load of 40 N in 3.5 wt.% NaCl solution are shown in Fig. 9. The SEM analyses reveal varying degrees of ploughing grooves on the wear tracks of Cr-0, Cr-1, Cr-2, and Cr-3. Comparatively, Cr-2 exhibits the narrowest scratch width of 350 µm after undergoing the longest duration of tribo-corrosion testing under the load of 40 N. The EDX spectra demonstrate the presence of a significant amount of Fe in the wear track, while only a minimal amount of C is observed, indicating wear of the GLC coating (Fig. 9(a, b, d)). In contrast to the Cr-0, Cr-1, and Cr-3 coatings, the surface of the Cr-2 coating appears highly smooth, with only a few cracks noticed at the edges of the wear track (Fig. 9(c)). More importantly, the carbon atoms are easily detected on the wear track surface, while the presence of Fe is minimal, indicating the integrity of the GLC coating. The phenomenon further confirms the excellent tribo-corrosion performance of Cr-2.

Fig. 10(a-c) exhibits the section profile of wear track and morphology of wear track edge of Cr-2 after tribo-corrosion test in 3.5 wt.% NaCl solution under the load of 40 N. It is evident that the depth of the wear track exceeds that of the GLC coating depicted in Fig. 2. That means the substrate 316L is exposed in the NaCl solution, due to the friction and corrosion damage. Throughout the tribo-corrosion process, the coating undergoes severe deformation, resulting in the appearance of cracks at the wear track's edge. Subsequently, Cl⁻ infiltrates the Cr interlayer, leading to galvanic corrosion and the formation of cavities within the Cr interlayer. This behavior aligns with our recent report [51], where the GLC coating ultimately collapses and eventually flakes off during long-term testing, as illustrated in Fig. 10(c). To further shed

light on the reasons why different Cr interlayer thicknesses lead to different erosion performance, the adhesion strength of Cr-1, Cr-2 and Cr-3 was obtained by the scratch tester with a progressive load. The results demonstrate that Cr-2 exhibits the highest adhesion strength at an approximate value of 29.2 N compared to Cr-1 and Cr-3. This phenomenon may be attributed to the interplay between the strain energy and surface energy of the interlayer with different thicknesses [37,52].

To delve deeper into the wear mechanisms of Cr/GLC films, the morphology of wear scars on the $\rm Si_3N_4$ ball after grinding with Cr-2 was examined, as depicted in Fig. 11. It can be clearly seen that the transferred tribo-films are formed on the $\rm Si_3N_4$ balls (Fig. 11(a, b)). Elemental analysis via EDX spectra (Fig. 11(c-e)) revealed that the transferred film primarily comprises carbon, which served as a lubricant during the sliding process, effectively reducing friction and wear [34,53]. Based on the aforementioned discussions, the Cr interlayer significantly enhances the tribo-corrosion resistance of GLC. Notably, an optimal thickness for the Cr interlayer enhances wear resistance under high-load conditions, rendering it suitable for marine components as a protective coating.

To elucidate the tribo-corrosion mechanism of the coatings under a 40 N load, a schematic illustration was devised and presented in Fig. 12. Based on the above analysis, under the load of 40 N, the coating deformed violently and cracks appeared at the edge of the wear track quickly (Fig. 12(b)). The preferential corrosion of the Cr interlayer weakens the binding between the GLC and the Cr interlayer. Consequently, the GLC coatings undergo delamination and ultimately fail (Fig. 12(c)). The interlayer assumes a critical role in determining the coating's load-bearing capacity, and an optimal Cr layer thickness confers the highest level of wear resistance.

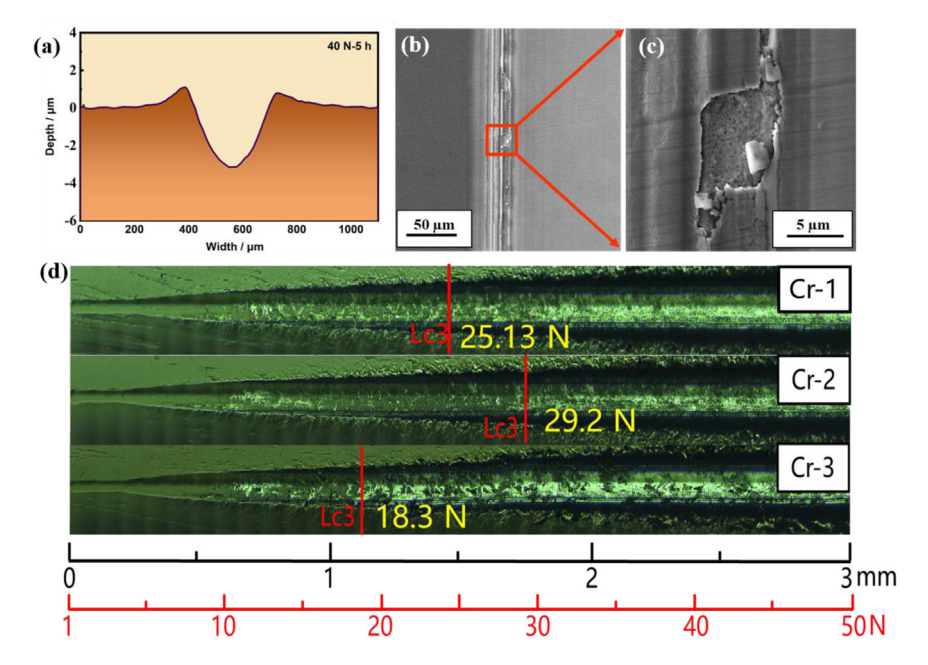
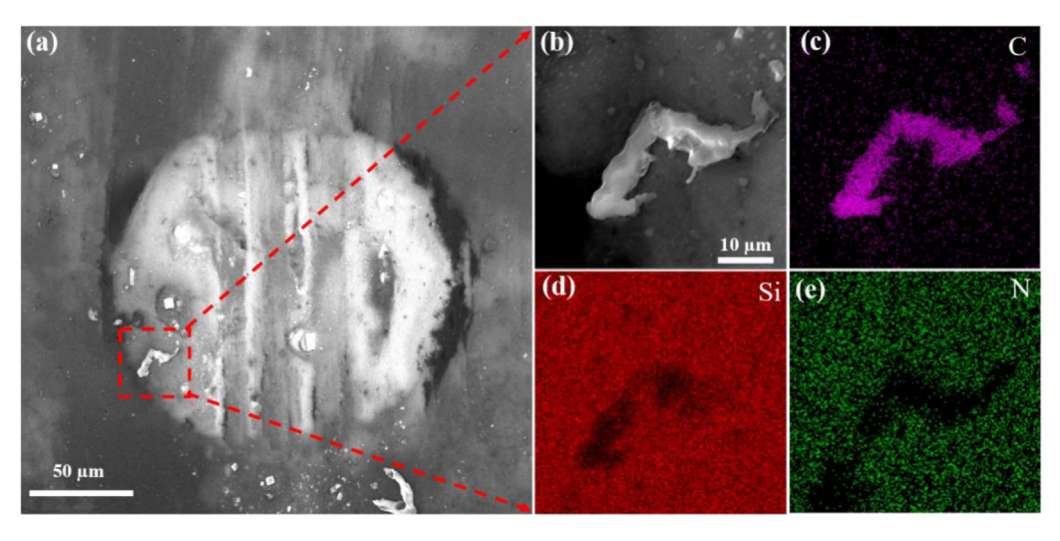


Fig. 10. (a) Profile of the wear track, (b, c) the edge morphology of wear track of Cr-2 after tribo-corrosion test, (d) scratch topography of Cr-1, Cr-2 and Cr-3.



 $\textbf{Fig. 11.} \ \ (a) \ \, \text{Morphology of wear track on Si}_3N_4 \ \, \text{ball, (b) high magnification of transfer film on Si}_3N_4 \ \, \text{ball, (c-e) EDX element mapping.}$

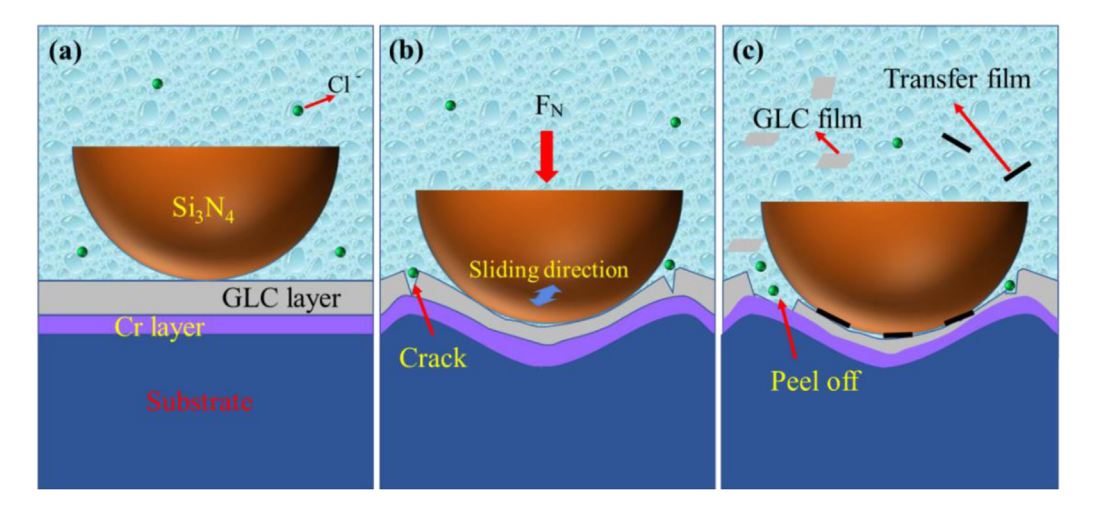


Fig. 12. Tribo-corrosion mechanism model in 3.5 wt.% NaCl solution: (a) Cr/GLC and Si_3N_4 in NaCl solution, (b) cracks appeared at the edge of the wear track, (c) the coatings began to peel off.

4. Conclusion and outlook

In this work, GLC coatings with varying thicknesses of Cr interlayer were successfully prepared on 316L by magnetron sputtering technology. The influence of Cr interlayer thickness on the microstructure, mechanical properties, and tribo-corrosion performance of the Cr/GLC coatings was systematically investigated. The results revealed that the addition and the thickness of Cr interlayers affect the sp²/sp³ ratio and the size of sp² clusters, respectively. All the GLC coatings exhibited a pronounced reduction in wear rate when tested in a 3.5 wt.% NaCl solution under a 5 N load. It was observed that the thickness of the Cr interlayer had minimal impact on the tribo-corrosion performance under these conditions, as the primary contributing factor was the surface characteristics of the GLC coating. However, the tribo-corrosion performance was significantly influenced by the thickness of the Cr interlayer under a higher load of 40 N, which was attributed to the crucial role played by the Cr interlayer in determining the adhesive strength and load-bearing capacity of the coating. The investigation underscores the importance of choosing an optimal Cr interlayer thickness to improve wear resistance in high-load scenarios. These findings offer a comprehensive insight into the electrochemical corrosion and tribological behavior of the GLC coatings, and suggest a promising approach for developing tailored protective coatings on 316L for marine applications.

No one method appears to work for all conditions. It has been confirmed that regulation of surface microstructure/composition by various technologies can improve the properties of structural materials, meanwhile, construction of surface pattern through surface texturing strategy can tailor their contact interface performance. In view of the complexity of service conditions in offshore equipment, the integrated structure and function of 316L on the surface are crucial to ensure service safety and lifetime. Therefore, textured surface covered by coating/film originated from material systems with different compositions and multiple functions, such as anti-corrosion, drag reduction and anti-fouling, would increasingly influence and enhance the performance of 316L for marine applications.

Declaration of competing interest

The authors declare that they have no known competing financial interests or personal relationships that could have appeared to influence the work reported in this paper.

CRediT authorship contribution statement

Guanshui Ma: Writing – review & editing, Methodology, Investigation, Funding acquisition, Formal analysis. Jiangshan Yan: Methodology, Investigation, Formal analysis. Naiming Lin: Writing – review & editing, Funding acquisition. Peng Guo: Writing – review & editing. Wei Yang: Methodology, Investigation. Changying Chen: Investigation. Aiying Wang: Writing – review & editing, Supervision, Project administration, Funding acquisition.

Acknowledgements

This work is financially supported by the Strategic Priority Research Program of the Chinese Academy of Sciences (XDB1210402), the National Science Fund for Distinguished Young Scholars of China (52025014), Natural Science Foundation of Ningbo (2023J410), Special Project of Science and Technology Cooperation and Exchange of Shanxi Province (202204041101021) and Central Government Guides Local Funds Project for Science and Technology Development of Shanxi Province (YDZJSX20231A018).

References

 S.N. Verichev, V.V. Mishakin, D.A. Nuzhdin, E.N. Razov, Experimental study of abrasive wear of structural materials under the high hydrostatic pressure, Ocean Eng. 99 (2015) 9–13.

- [2] W. Quan, Y. Liu, Z. Zhang, X. Li, C. Liu, Scale model test of a semi-active heave compensation system for deep-sea tethered ROVs, Ocean Eng. 126 (2016) 353–363.
- [3] T. Duan, W. Peng, K. Ding, W. Guo, J. Hou, W. Cheng, S. Liu, L. Xu, Long-term field exposure corrosion behavior investigation of 316L stainless steel in the deep-sea environment, Ocean Eng. 189 (2019) 106405.
- [4] L.W. Wang, Y. Ding, Z. Guo, Y.X. Liu, Z.Y. Cui, Microstructure and corrosion behavior of welded joint between 2507 superduplex stainless steel and E690 low alloy steel, Corros. Commun. 11 (2023) 1–11.
- [5] P. Ren, H. Meng, Q. Xia, Z. Zhu, M. He, Tribo-corrosion of 316L stainless steel by in-situ electrochemical methods under deep-sea high hydrostatic pressure environment, Corros. Sci. 202 (2022) 110315.
- [6] M. Łępicka, M. Grądzka-Dahlke, D. Pieniak, K. Pasierbiewicz, A. Niewczas, Effect of mechanical properties of substrate and coating on wear performance of TiN- or DLC-coated 316LVM stainless steel, Wear 382 (2017) 62–70.
- [7] Y. Uzun, Tribo-corrosion properties of plasma nitrided, Ti-DLC coated and duplex surface treated AISI 316L stainless steel, Surf. Coat. Technol. 441 (2022) 128587.
- [8] W.L. Ma, H.D. Guo, L. Cai, X. Li, Y. Hua, A synergistic experimental and computational study on CO₂ corrosion of X65 carbon steel under dispersed droplets within oil-water mixture, Corros. Commun. 12 (2023) 34–75.
- [9] F. Ma, J. Li, Z. Zeng, Y. Gao, Tribo-corrosion behaviour of F690 and 316L steel in artificial seawater, Lubr. Sci. 30 (2018) 365–375.
- [10] Y. Zhang, H. Li, L. Cui, W. Yang, G. Ma, R. Chen, P. Guo, P. Ke, A. Wang, Comparative study on tribo-corrosion behavior of hydrogenated/hydrogen-free amorphous carbon coated WC-based cermet in 3.5 wt % NaCl solution, Corros. Sci. 227 (2024) 111738.
- [11] R. Shi, Y. Tu, K. Gao, L. Qiao, X. Pang, High stress corrosion cracking resistance of in-situ nanoparticle strengthened steel, Corros. Commun. 5 (2022) 14–24.
- [12] Y. Liu, L. Liu, S. Li, R. Wang, P. Guo, A. Wang, P.L. Ke, Accelerated deterioration mechanism of 316L stainless steel in NaCl solution under the intermittent tribo-corrosion process, J. Mater. Sci. Technol. 121 (2022) 67–79.
- [13] E. Liu, Y. Zhang, L. Zhu, Z. Zeng, R. Gao, Effect of strain-induced martensite on the tribo-corrosion of AISI 316L austenitic stainless steel in seawater, RSC Adv. 7 (2017) 44923–44932.
- [14] H. Li, L. Liu, P. Guo, L. Sun, J. Wei, Y. Liu, S. Li, S. Wang, K.R. Lee, P. Ke, A. Wang, Long-term tribo-corrosion resistance and failure tolerance of multilayer carbon-based coatings, Friction 10 (2022) 1707–1721.
- [15] X. Zhou, Y. Zhang, P. Guo, L. Cui, A. Wang, P. Ke, Tribological behavior of Cr/a-C multilayered coating against PEEK under dry sliding condition, Wear (2023) 204625 518-519
- [16] X.W. Li, N.Z. Du, C. Feng, K. Chen, X. Wei, D. Zhang, K.-R. Lee, Theoretical superlubricity and its friction stability of amorphous carbon film induced by simple surface graphitization, Appl. Surf. Sci. 615 (2023) 156318.
- [17] N.Z. Du, X.W. Li, X. Wei, Z. Chen, S. Lu, J. Ding, C. Feng, K. Chen, J. Qiao, D. Zhang, K.R. Lee, Atomistic insights into interfacial optimization mechanism for achieving ultralow-friction amorphous carbon films under solid-liquid composite conditions, ACS Appl. Mater. Interfaces 15 (2023) 53122–53135.
- [18] M. Gao, W. Lu, B. Yang, S. Zhang, J. Wang, High corrosion and wear resistance of Al-based amorphous metallic coating synthesized by HVAF spraying, J. Alloy. Compd. 735 (2018) 1363–1373.
- [19] D. Zhang, X. Zuo, Z. Wang, H. Li, R. Chen, A. Wang, P. Ke, Comparative study on protective properties of CrN coatings on the ABS substrate by DCMS and HiPIMS techniques, Surf. Coat. Technol. 394 (2020) 125890.
- [20] Z.C. Li, Z. Wang, G.S. Ma, R. Chen, W. Yang, K. Wang, P. Ke, A. Wang, High-performance Cr₂AlC MAX phase coatings for ATF application: interface design and oxidation mechanism, Corros. Commun. 13 (2024) 27–36.
- [21] A.A. Al-Azizi, O. Eryilmaz, A. Erdemir, S.H. Kim, Nano-texture for a wear-resistant and near-frictionless diamond-like carbon, Carbon 73 (2014) 403–412.
- [22] M.M. Yan, X. Wang, S. Zhang, S. Zhang, X. Sui, W. Li, J. Hao, W. Liu, Friction and wear properties of GLC and DLC coatings under ionic liquid lubrication, Tribol. Int. 143 (2020) 106067.
- [23] S.Y. Li, H. Li, Y. Zhang, W. Yang, P. Guo, X. Li, K. Nishimura, P.L. Ke, A.Y. Wang, Dense Al₂O₃ sealing inhibited high hydrostatic pressure corrosion of Cr/GLC coating, npj. Mater. Degrad. 8 (2024) 48.
- [24] S.K. Field, M. Jarratt, D.G. Teer, Tribological properties of graphite-like and diamond-like carbon coatings, Tribol. Int. 37 (2004) 949–956.
- [25] S.Y. Li, H. Li, J. Wei, G.S. Ma, R.D. Chen, K. Nishimura, P. Guo, P. Ke, A.Y. Wang, Nodular defects aggravated tribo-corrosion failure mechanism in Cr/GLC multilayer coatings for marine applications, J. Mater. Res. Technol. 30 (2024) 6470–6481.
- [26] N.Z. Du, X.B. Wei, X.W. Li, Z. Chen, S. Lu, J. Ding, C. Feng, K. Chen, J. Qiao, D. Zhang, K.R. Lee, Unraveling the friction response from selective hydrogenation of textured amorphous carbon surface, Appl. Surf. Sci. 614 (2023) 156246.
- [27] J. Li, H. Hong, L. Sun, Y. Yang, D. Li, S. Zhang, Argon ion sputtering bridging plasma nitriding and GLC film deposition: effects on the mechanical and tribological properties, Surf. Coat. Technol. 479 (2024) 130559.
- [28] X. Sui, R. Xu, J. Liu, S. Zhang, Y. Wu, J. Yang, J. Hao, Tailoring the tribo-corrosion and antifouling performance of (Cr, Cu)-GLC coatings for marine application, ACS Appl. Mater. Interfaces 10 (2018) 36531–36539.
- [29] N.W. Khun, E. Liu, X.T. Zeng, Corrosion behavior of nitrogen doped diamond-like carbon thin films in NaCl solutions, Corros. Sci. 51 (2009) 2158–2164.
- [30] X.W. Xu, Y. Zhou, L. Liu, P. Guo, X. Li, K.-R. Lee, P. Cui, A.Y. Wang, Corrosion behavior of diamond-like carbon film induced by Al/Ti co-doping, Appl. Surf. Sci. 509 (2020) 144877.
- [31] T. Borowski, K. Kulikowski, B. Adamczyk-Cieślak, K. Rożniatowski, M. Spychalski, M. Tarnowski, Influence of nitrided and nitrocarburised layers on the functional properties of nitrogen-doped soft carbon-based coatings deposited on 316L steel under DC glow-discharge conditions, Surf. Coat. Technol. 392 (2020) 125705.

- [32] D. Liu, T. Yang, H. Ma, Y. Liang, The microstructure, bio-tribological properties, and biocompatibility of titanium surfaces with graded zirconium incorporation in amorphous carbon bioceramic composite films, Surf. Coat. Technol. 385 (2020) 125391.
- [33] Y. Wang, L. Wang, Q. Xue, Controlling wear failure of graphite-like carbon film in aqueous environment: two feasible approaches, Appl. Surf. Sci. 257 (2011) 4370–4376.
- [34] W.Q. Wang, X. Ling, R. Wang, W. Nie, L. Ji, H. Li, Structure and characterization of TiC/GLC multilayered films with various bilayers periods, Coatings 11 (2021) 787.
- [35] H. Li, Y. Xin, K. Komatsu, P. Guo, G. Ma, P. Ke, K.R. Lee, H. Saito, A. Wang, Controlling the compactness and sp² clusters to reduce interfacial damage of amorphous carbon/316L bipolar plates in PEMFCs, Int. J. Hydrog. Energy 47 (2022) 11622–11632.
- [36] Y. Jeon, Y.S. Park, H.J. Kim, B. Hong, W.S. Choi, Tribological properties of ultrathin DLC films with and without metal interlayers, J. Korean Phys. Soc. 51 (2007) 1124–1128
- [37] X. Shi, Y. Shi, J. Chen, T.W. Liskiewicz, B.D. Beake, Z. Zhou, Z. Wang, G. Wu, Influence of gradient interlayer thickness on corrosion and tribological behavior of Ti-containing multilayer graphite-like carbon films, Wear 488-489 (2022) 204177.
- [38] Q. Chen, C. Zeng, M. Xu, H. Yuan, H. Lv, Z. Wang, X. Wang, Effect of SiN interlayer thickness on adhesion and friction properties of diamond-like carbon films, Diamond Relat. Mater. 94 (2019) 186–193.
- [39] Y. Wang, J. Pu, J. Wang, J. Li, J. Chen, Q. Xue, Interlayer design for the graphite-like carbon film with high load-bearing capacity under sliding-friction condition in water, Appl. Surf. Sci. 311 (2014) 816–824.
- [40] L. Li, P. Guo, L.L. Liu, X. Li, P.L. Ke, A.Y. Wang, Structural design of Cr/GLC films for high tribological performance in artificial seawater: Cr/GLC ratio and multilayer structure, J. Mater. Sci. Technol. 34 (2018) 1273–1280.
- [41] L. Li, G. Peng, L.L. Liu, L.L. Sun, P.L. Ke, A.Y. Wang, Metal buffer layer on structure, mechanical and tribological property of GLC films, J. Inorg. Mater. 3 (2018) 331–338
- [42] L.C. Bai, G. Zhang, Z. Lu, Z. Wu, Y. Wang, L. Wang, P. Yan, Tribological mechanism of hydrogenated amorphous carbon film against pairs: a physical description, J. Appl. Phys. 110 (2011) 033521.

- [43] W.S. Hincapie C, J.M. Gutiérrez B, V.J. Trava-Airoldi, J.J. Olaya F, J.E. Alfonso, G. Capote, Influence of the TixSi and TixSi/a-Si: h interlayers on adherence of diamond-like carbon coatings, Diamond Relat. Mater. 109 (2020) 108079.
- [44] F. Shahsavari, M. Ehteshamzadeh, M.R. Naimi-Jamal, A. Irannejad, Nanoindentation and nanoscratch behaviors of DLC films growth on different thickness of Cr nanolayers, Diamond Relat. Mater. 70 (2016) 76–82.
- [45] P. Guo, X. Li, L. Sun, R. Chen, P. Ke, A. Wang, Stress reduction mechanism of diamond-like carbon films incorporated with different Cu contents, Thin Solid Films 640 (2017) 45–51.
- [46] X. Shi, T.W. Liskiewicz, B.D. Beake, Z. Sun, J. Chen, Fretting wear behavior of graphite-like carbon films with bias-graded deposition, Appl. Surf. Sci. 494 (2019) 929–940.
- [47] X.W. Li, L. Li, D. Zhang, A.Y. Wang, Ab initio study of interfacial structure transformation of amorphous carbon catalyzed by Ti, Cr, and W transition layers, ACS Appl. Mater. Interfaces 9 (2017) 41115–41119.
- [48] K.M. Lee, H.J. Han, S. Choi, K.H. Park, K.H. Koh, Effects of metal buffer layers on the hot filament chemical vapor deposition of nanostructured carbon films, J. Vac. Sci. Technol. B 21 (2003) 623–626.
- [49] D. Dong, B. Jiang, H. Li, Y. Du, C. Yang, Effect of graphite target power density on tribological properties of graphite-like carbon films, Appl. Surf. Sci. 439 (2018) 900–909
- [50] Y. Ye, C. Wang, H. Chen, Y. Wang, J. Li, F. Ma, An analysis of the tribological mechanism of GLC film in artificial seawater, RSC Adv. 6 (2016) 32922–32931.
- [51] S.Y. Li, H. Li, G.S. Ma, J. Wei, G.X. Zhou, Y. Zhang, P. Guo, P.L. Ke, A.Y. Wang, Dense Cr/GLC multilayer coating by HiPIMS technique in high hydrostatic pressure: microstructural evolution and galvanic corrosion failure, Corros. Sci. 225 (2023) 111618
- [52] G.S. Ma, D. Zhang, P. Guo, H. Li, Y. Xin, Z.Y. Wang, A.Y. Wang, Phase orientation improved the corrosion resistance and conductivity of Cr₂AlC coatings for metal bipolar plates, J. Mater. Sci. Technol. 105 (2022) 36–44.
- [53] Y. Zhang, Z. Wang, S. Zhou, Y. Zhang, Y. Dong, A. Wang, P. Ke, Synergistic effect of V and Ag diffusion favored the temperature-adaptive tribological behavior of VAIN/Ag multi-layer coating, Tribol. Int. 192 (2024) 109285.